Tectonophysics 689 (2016) 67–78

Contents lists available at ScienceDirect

Tectonophysics

journal homepage: www.elsevier.com/locate/tecto

Dynamic seismic response of a stable intraplate region to a megathrust earthquake

Soung Eil Houng, Junhyung Lee, Tae-Kyung Hong *

Yonsei University, Department of Earth System Sciences, 50 Yonsei-ro, Seodaemun-gu, Seoul 120-749, South Korea

ARTICLE INFO

Article history:
Received 6 July 2015
Received in revised form 26 July 2016
Accepted 29 July 2016
Available online 30 July 2016

Keywords:
Dynamic triggering
Megathrust earthquake
Seismicity
Stable intraplate region
Omori law

ABSTRACT

The 2011 M9.0 Tohoku-Oki megathrust earthquake produced strong ground motions with a peak ground acceleration of 1.52 cm/s ^{2} in the Korean Peninsula, inducing large dynamic-stress changes in the crust. Sixty-one triggered earthquakes with magnitudes of 0.5–2.5 including 17 unusual, spatially-clustered events were identified from continuous seismic record sections of dense seismic networks for 18 h following the megathrust earthquake. The triggered earthquakes occurred in regions of high seismicity. The earthquake occurrence frequency increased after the megathrust earthquake, keeping the Gutenberg-Richter *b* value invariant. The seismic occurrence rates decreased with time following a modified Omori law. The focal mechanism solutions of triggered earthquakes are consistent with those observed before the megathrust earthquake. An unusual earthquake swarm displays apparent migration with a speed of 28.6 ± 4.4 m/h. The changes in pore fluid pressure induced by strong seismic waves may have caused the triggering of earthquakes. The duration and strength of dynamic triggering may be highly dependent on the magnitude and distance of megathrust earthquake.

1. Introduction

Earthquakes can occur as a consequence of stress change in a medium. Coseismic and postseismic deformation produces a static stress change that depends on the fault geometry and distance (King et al., 1994; Stein, 1999; Kilb et al., 2002; Parsons et al., 2008). It was reported that a static stress change at a distance less than a few fault lengths can induce earthquakes, and a strong positive correlation between static stress change and post-event seismicity was found (Freed, 2005). The static stress change could be quantified through the change in a Coulomb failure function (e.g., Reasenberg and Simpson, 1992). The seismicity generally increases in a region of static-stress increase, and it decreases in a region of static-stress decrease (stress shadows) (e.g., Reasenberg and Simpson, 1992; Freed and Lin, 2001). Earthquake triggering caused by a static stress change is observed in various environments including plate boundaries, volcanic and geothermal areas and stable intraplate regions (e.g., Stein et al., 1992; Bohnenstiehl et al., 2002; Asano et al., 2011).

Strong ground motions can produce a large dynamic stress change in the medium (e.g., Tibi et al., 2003; Freed, 2005; Hill and Prejean, 2007), inducing subcritical crack growth (Atkinson, 1984), changes in medium properties (Johnson and Jia, 2005; Parsons, 2005), and pore-pressure change (Hill et al., 1993; Brodsky et al., 2003). The dynamic stress change is responsible for the remote triggering of earthquakes in regional and teleseismic distances in which the static stress change is not effective (e.g., Hill and Prejean, 2007; Gonzalez-Huizar et al., 2012). The dynamically triggered earthquakes have typically small magnitudes (Hill and Prejean, 2007; Parsons and Velasco, 2011). The dynamic triggering of earthquakes lasts for a few minutes to several weeks (Knopoff and Gardner, 1972; Hill and Prejean, 2007). The dynamic triggering is not only observed in active tectonic regions, but also in stable regions (e.g., Hill et al., 1993; Brodsky et al., 2000; Hough, 2001; Hough et al., 2003; Saccorotti et al., 2013; Tibi et al., 2003; Pankow et al., 2004; Miyazawa and Mori, 2005; West et al., 2005; Velasco et al., 2008; Jiang et al., 2010; Yukutake et al., 2013).

A megathrust earthquake produces large coseismic and postseismic lithospheric deformations, incorporating a large number of aftershocks (e.g., Takahashi, 2011; Toda et al., 2011; Lee and Hong, 2014). Large megathrust earthquakes triggered earthquakes over the globe in various tectonic environments (e.g., Hough et al., 2003; Gomberg et al., 2004; Velasco et al., 2008; Peng et al., 2010; Gonzalez-Huizar and Velasco, 2011; Wu et al., 2011; Miyazawa, 2011; Yukutake et al., 2011; Gonzalez-Huizar et al., 2012). The earthquake triggering temporally increases the seismicity, which is particularly crucial for the assessment of seismic hazard potentials in intraplate regions with long earthquake-recurrence intervals. We investigate the properties of dynamically triggered earthquakes around the Korean Peninsula after the 2011 M9.0 Tohoku-Oki earthquake.

* Corresponding author.
E-mail address: tkhong@yonsei.ac.kr (T.-K. Hong).

http://dx.doi.org/10.1016/j.tecto.2016.07.033
0040-1951/

2. Geology and seismicity

The Korean Peninsula is located on the far-eastern Eurasian plate, and belongs to a stable intraplate regime (Fig. 1). The current shapes of the Korean Peninsula and East Sea (Sea of Japan) were formed after consecutive tectonic evolutions of a continental collision between the North and South China blocks from the late Permian to the Jurassic and after continental rifting from the Oligocene to the mid-Miocene (Jolivet et al., 1994; Chough et al., 2000; Oh, 2006). The surface of the Korean Peninsula is composed of three Precambrian massifs (Nangrim, Gyeonggi, and Yeongnam), two Permo-Triassic orogenic belts (Imjingang and Okcheon), two Paleozoic sedimentary basins (Pyeongnam and Taebaeksan), and a Cretaceous volcanic-sedimentary basin (Gyeongsang) (Fig. 1(b)) (Choi, 1986; Chough et al., 2000; Oh, 2006; Ernst et al., 2007). The orogeny from the late Paleozoic to the Mesozoic formed NE-trending geological structures (Chough et al., 2000). The geological and tectonic structures present distinct seismic properties (Kang and Shin, 2006; Hong and Kang, 2009; Choi et al., 2009; Hong, 2010; Jo and Hong, 2013).

The crust of the inland peninsula and Yellow Sea presents the properties of continental crust with a thickness of 28–38 km (Pasyanos et al., 2006; Chang and Baag, 2006; Hong et al., 2008). On the other hand, the East Sea displays a transitional structure between continental and oceanic crusts (Hirata et al., 1989; Kim et al., 1998; Sato et al., 2006; Hong, 2010; Kulinich and Valitov, 2011). The Japan basin in the central East Sea is composed of oceanic crust with a thicknesses of 8.5–14 km. The tectonic setting around the Korean Peninsula forms the ambient stress field of ENE-directional compression and SSE-directional tension (Choi et al., 2012).

The seismicity is distributed over the peninsula with some regional localizations in the southern and northwestern peninsula and the offshore regions of the southeast and west coasts (Choi et al., 2012; Hong and Choi, 2012; Houng and Hong, 2013). The largest magnitude of events observed around the peninsula since 1978, the year in which national seismic monitoring began, was M_L5.3. The largest instrumentally recorded event occurred at the northwestern peninsula in 1952, the magnitude of which was M_S6.5 (Engdahl and Villasenor, 2002). Historical earthquake records suggest that there were several earthquakes with magnitudes of ~7.0 in the last 600 years (Houng and Hong, 2013). Strike-slip earthquakes are the most dominant around the peninsula. Normal-faulting earthquakes occur around the paleo-continental-collision region in the Yellow Sea (Hong and Choi, 2012). We observe thrust events in the paleo-rifting region off the east coast of the peninsula (Choi et al., 2012). The earthquakes concentrate at depths of 5–15 km, although they can reach up to 35 km (Chen and Molnar, 1983; Hong and Choi, 2012).

3. Data

The 11 March 2011 M9.0 Tohoku-Oki earthquake occurred at the convergent boundary between the Pacific and Okhotsk plates, rupturing a ~440-km-long and ~180-km-wide zone along the plate interface for ~150 s (Yagi and Fukahata, 2011). The coseismic slips reached 30–60 m at the hypocenter and trench (Lay et al., 2011; Tajima et al., 2013). The coseismic slip was large near the trench, which developed a huge tsunami. The peak ground acceleration in Kurihara city in Miyagi prefecture, southeastern Tohoku region reached ~3 g, which is equivalent to seismic intensity X in the modified Mercalli intensity scale (Hoshiba et al., 2011; Irikura and Kurahashi., 2012; Peng et al., 2012). The run-up height of the tsunami reached ~40 m at the nearest coast from the epicenter (Mori et al., 2011). A large number of aftershocks followed the megathrust earthquake around the rupture zone (e.g., Takahashi, 2011; Toda et al., 2011; Lee and Hong, 2014).

The Korean Peninsula is located at distances of 1100 to 1500 km (about 3 times the fault length) from the epicenter of the 2011 Tohoku-Oki earthquake (Fig. 1). The peninsula was dislocated to the epicenter by 2–5 cm (Baek et al., 2012; Kim and Bae, 2012; Zhou et al., 2012). The groundwater level changed abruptly by ~110 cm (Lee and Woo, 2012; Lee et al., 2013). Seismic stations are densely distributed over the Korean Peninsula (Fig. 1). Strong seismic waves from the megathrust earthquake are observed in the Korean Peninsula. Continuous seismic waveform record sections for 2 h before and 18 h after the Tohoku-Oki earthquake were collected from 135 stations in the Korean Peninsula (Fig. 2). The average inter-station distance is 20.3 km. The seismic stations are composed of 41 broadband and 35 short-period velocity seismometers and 59 accelerometers. The sampling rate of record sections is 100 Hz.

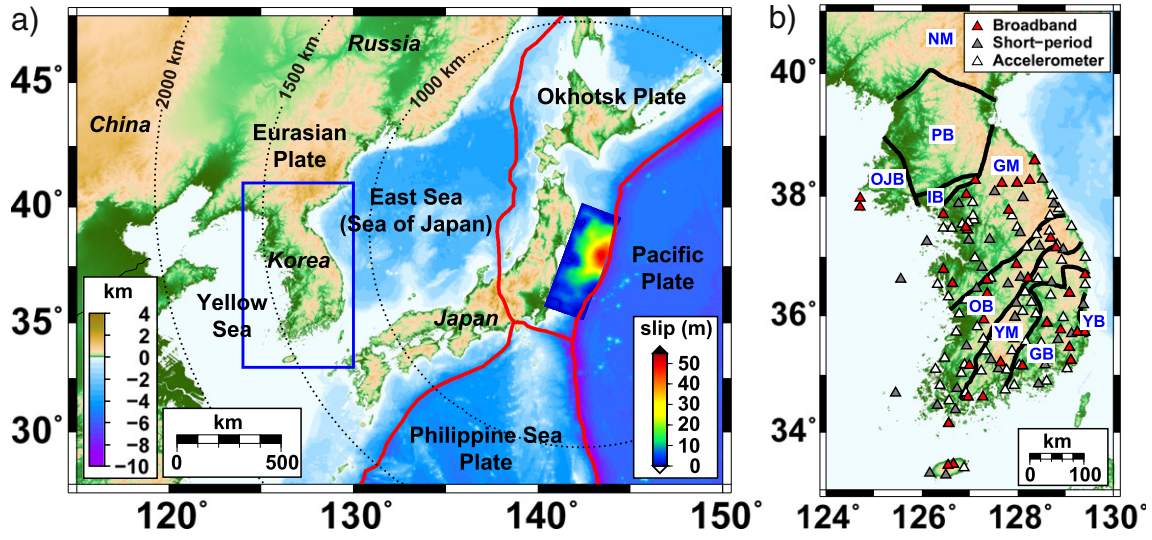

Fig. 1. (a) Map of the region around the eastern Eurasian plate. A source slip model of the 2011 M9.0 Tohoku-Oki earthquake (Yagi and Fukahata, 2011) and plate boundaries are presented. (b) An enlarged map of the region around the Korean Peninsula with major geological structures (solid lines) and seismic stations (triangles). The stations are equipped with velocity seismometers (broadband or short-period), or accelerometers. The major geological provinces include Gyeonggi massif (GM), Gyeongsang basin (GB), Imjingang belt (IB), Nangnim massif (NM), Okcheon belt (OB), Ongjin basin (OJB), Pyeongnam basin (PB), Yeonil basin (YB), and Yeongnam massif (YM).

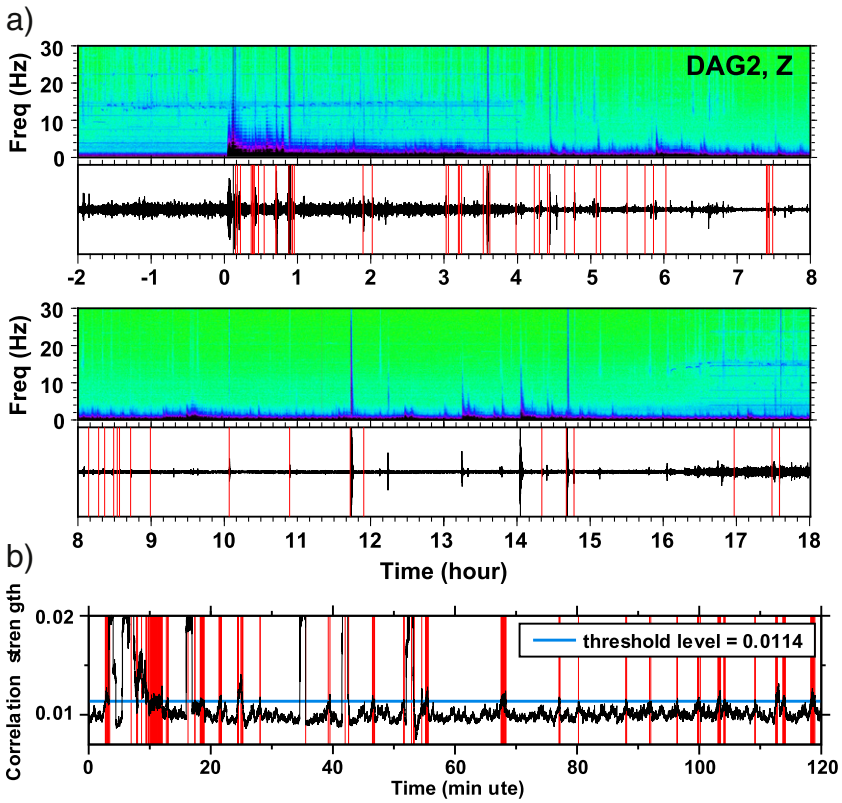

Fig. 2. (a) Spectrogram of vertical velocity waveforms at station DAG2 for 2 h before and 18 h after the megathrust earthquake. The vertical velocity waveforms bandpass-filtered between 5 and 20 Hz are presented for comparison. The origin times of 61 detected earthquakes are marked with vertical lines on the record sections. No events were observed before the megathrust earthquake. (b) An example of event detection based on an automated detection algorithm for 2 h after the megathrust earthquake. Event detection is assumed when the correlation strength is greater than an empirical threshold level (horizontal solid line).

We find strong ground motions by seismic waves from the megathrust earthquake. The peak ground accelerations (PGA) and velocities (PGV) that are calculated by the square root of the sum of squares of zero-to-peak amplitudes in three components reached 0.11–1.52 cm/s ^{2} and 0.40–4.60 cm/s in frequencies of 0.05–20 Hz (Fig. 3). The great-circle directions between the megathrust earthquake and events are nearly subparallel with the compression axis of the ambient stress field.

We additionally collect seismic waveforms for 650 local earthquakes from 2001 to 2013 to calculate the reference traveltime curves of *P* and *S* waves around the peninsula. The magnitudes of the events are 1.7–5.2, and the focal depths are less than 30 km. The event information was

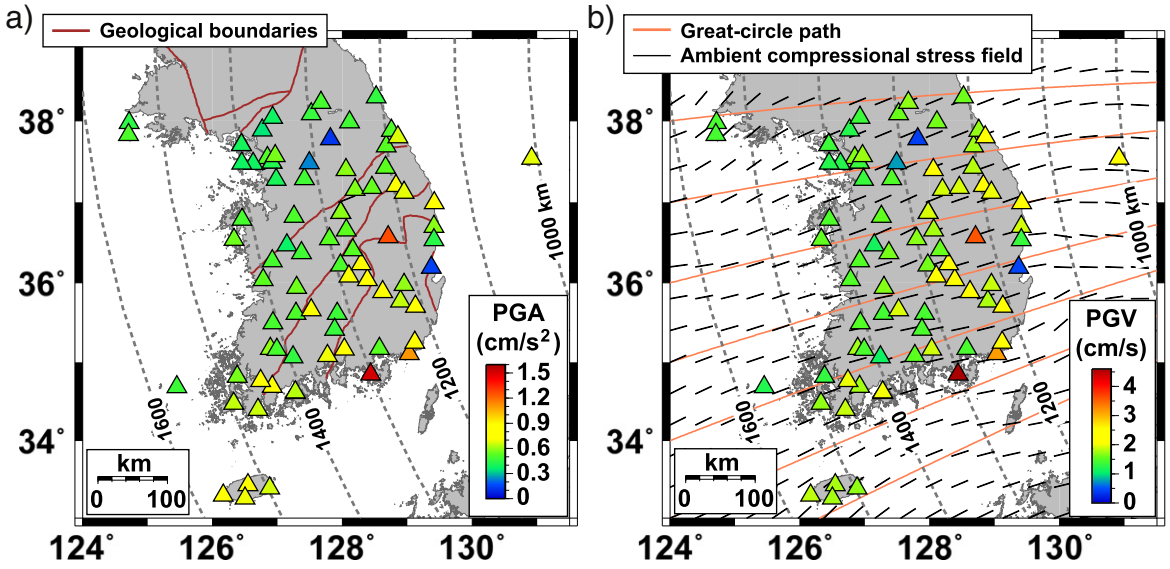

Fig. 3. Strong ground motions induced by the 2011 Tohoku-Oki earthquake: (a) peak ground accelerations (PGAs) and (b) peak ground velocities (PGVs) observed in the Korean Peninsula. The PGAs range between 0.11 and 1.52 cm/s ^{2}, and the PGVs are 0.40–4.60 cm/s in the frequency band between 0.05 and 20 Hz. The orientations of the maximum horizontal compressive stresses (Choi et al., 2012) are indicated by line segments.

collected from the Korea Meteorological Administration (KMA) and the Korea Institute of Geoscience and Mineral Resources (KIGAM).

4. Methods

4.1. Event detection and determination of hypocentral parameters

The seismic signals from micro or small events are naturally weak. It is difficult to identify seismic phases from a weak wavefield with a conventional method, increasing the detection difficulty of small events. We implement a method based on multiple-station wavetrains to determine the phase arrival times and event location jointly. The method tests the possible occurrence of an event at an assumed location and origin time by examining the observation of seismic energy at the expected *P* and *S* arrival times (Withers et al., 1999). The event occurrence is recognized by the agreement between the reference seismic traveltimes and seismic wavetrains.

We prepare sets of source locations and event origin times and determine an optimum set of source location and event origin time satisfying the traveltimes. The agreement between the reference seismic traveltimes and seismic wavetrains is assessed through a correlation matrix **C** given by

$$\mathbf{C} = \mathbf{MD} \tag{1}$$

where **M** is an *I*-by-*K* matrix for reference traveltimes, **D** is a *K*-by-*J* matrix for observed record sections, *I* is the number of discrete distances, *K* is the number of discrete times, and *J* is the number of stations. When a seismic phase (*P* or *S*) arrives in a discrete time bin *k* from an event at a distance of *i*, we set element M_{ik} to be 1. Else, element M_{ik} is set to be zero. Element D_{kj} is the ratio between the short-term average amplitude and long-term average amplitude of waveforms (STA/LTA) at station *j* in discrete time *k*. Element C_{ij} presents the probability of event occurrence at a discrete distance *i* from station *j*.

We define the correlation index, $\xi(l,t)$, for an event that occurs at the origin time *t* at location *l*:

$$\xi(l,t) = \frac{1}{J}\sum_{j=1}^{J} C_{ij}(l,t) \tag{2}$$

where $C_{ij}(l,t)$ is an element of the correlation matrix for an event with location *l* and origin time *t*. A pair of event location and origin time yielding the peak correlation magnitude is selected to be probable source parameters. When the correlation magnitude is greater than a prescribed value, we declare event detection. In this study, we set the prescribed value to be 4 times the median of observed correlation indices. The threshold level approximately corresponds to 2.7 times the standard deviation of a data set in normal distribution, resulting in an event declaration for every 300 data samples. The threshold level can be adjusted considering the level of ambient noise. The procedure is applied to full waveform records.

After event recognition, the event location is determined by a traditional hypocentral parameter inversion method, HYPOINVERSE that is based on *P* and *S* arrival times (Klein, 2002). The hypocenters of events clustered in a small area are further refined using a double difference location algorithm (Waldhauser and Ellsworth, 2000).

We finally determine the magnitudes of detected events. There are several local magnitude scales for the Korean Peninsula (e.g., Hong et al., 2000; Kim and Park, 2005). In this study, we implement a local magnitude scale applicable to events with weak signals (Tsuboi, 1954; Tsumura, 1967)

$$M_L = 0.5\log\left(A_N{}^2 + A_E{}^2\right) + 1.73\log\Delta - 0.83 \tag{3}$$

where A_N and A_E are the zero-to-peak NS- and EW-directional displacements in μm, respectively, and Δ is the epicentral distance in km.

4.2. Dynamic stress changes

Transient seismic waves produce the peak dynamic strain that can be approximated to be the peak particle velocity divided by the phase velocity (e.g., Hill and Prejean, 2007). The peak magnitude of dynamic shear strain ε_m induced by the dominant shear wave can be calculated by

$$\varepsilon_m = \frac{\dot{U}_m}{V_s} \tag{4}$$

where $\dot{U}_m$ is the peak ground velocity (PGV), and V_s is the shear wave velocity. The PGV is determined to be the peak absolute amplitude of ground velocity. The peak dynamic stress change, σ_m, associated with the peak dynamic strain is given by

$$\sigma_m = \mu\frac{\dot{U}_m}{V_s} \tag{5}$$

where μ is the shear modulus.

4.3. Statistical analysis of seismicity properties

The seismicity of any region presents a characteristic feature to satisfy a unique magnitude-dependent earthquake occurrence rate. The Gutenberg-Richter frequency-magnitude relationship is given by

$$\log N = a - bM, \tag{6}$$

where *M* is the magnitude, and *N* is the annual number of earthquakes with magnitudes equal to or greater than *M*. Constants *a* and *b* are determined by the maximum likelihood method (Tinti and Mulargia, 1987; Shcherbakov et al., 2013).

The number of aftershocks generally decreases with time, following a modified Omori law (Utsu et al., 1995):

$$r(t) = \frac{K}{(t+c)^p}, \tag{7}$$

where $r(t)$ is the number of aftershocks per unit time, and *t* is the time elapsed (in hours) after the mainshock. We determine a set of

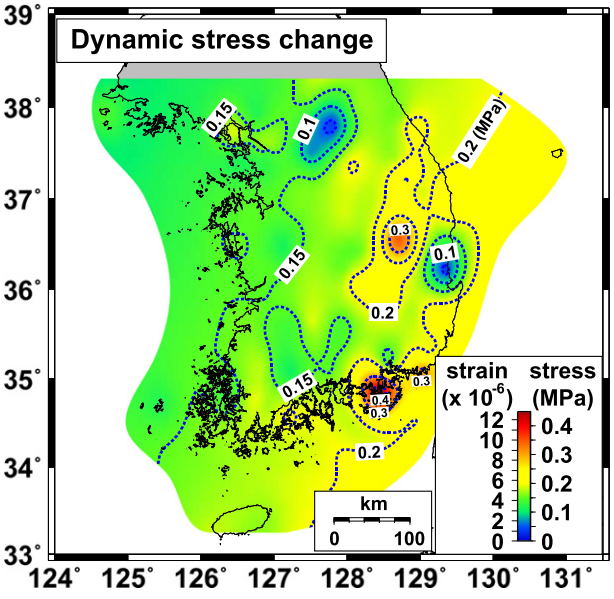

Fig. 4. Peak dynamic shear strains and stresses induced by transient seismic waves. The peak magnitudes of dynamic shear stress reach 0.449 MPa in the inland region.

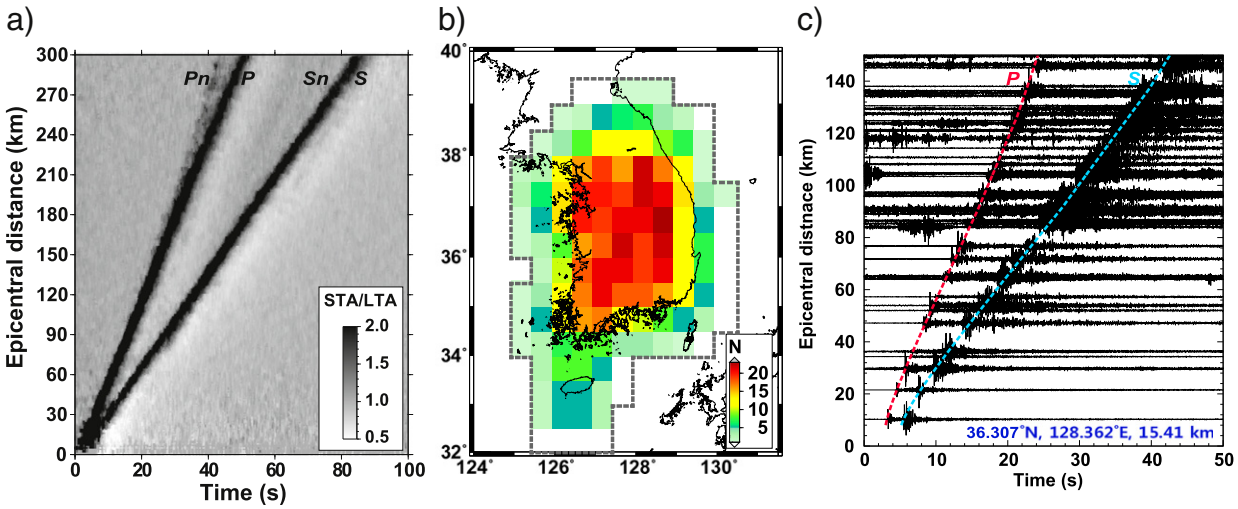

Fig. 5. (a) Stacked STA/LTA estimates. The *P* and *S* arrivals are well illuminated. The mantle-lid phases (*Pn, Sn*) develop in epicentral distances greater than ~150 km. (b) The number of stations in discrete spatial bins with a uniform size of $1.5^{\circ}\times1.5^{\circ}$. Each bin overlaps with neighboring bins by 1.0° in both latitude and longitude. Regions with numbers of stations greater than or equal to 5 are analyzed. (c) An example of seismic waveforms of a detected event in 36.307 °N and 128.362 °E. The focal depth is 15.41 km. The *P* and *S* phase arrivals match well with the theoretical travel time curves.

parameters K, c, and p maximizing a log-likelihood function, log$L$ of aftershock sequence (Ogata, 1999; Shcherbakov et al., 2013):

$$\log L = N_e \log K - p\sum_{i=1}^{N_e} \log(t_i + c) - \Lambda(K, c, p; t_a, t_b) \tag{8}$$

where N_e is the number of aftershocks with magnitudes greater than or equal to M_e, t_i is the origin time of the ith aftershock, t_a and t_b are the beginning and ending times of aftershock sequence, and Λ is the predicted number of earthquakes for the period from t_a to t_b. Function Λ is given by

$$\Lambda(K, c, p; t_a, t_b) = \begin{cases} \dfrac{K}{1-p}\left[(t_b + c)^{1-p} - (t_a + c)^{1-p}\right], & \text{for } p \neq 1 \\ K[\log(t_b + c) - \log(t_a + c)], & \text{for } p = 1. \end{cases} \tag{9}$$

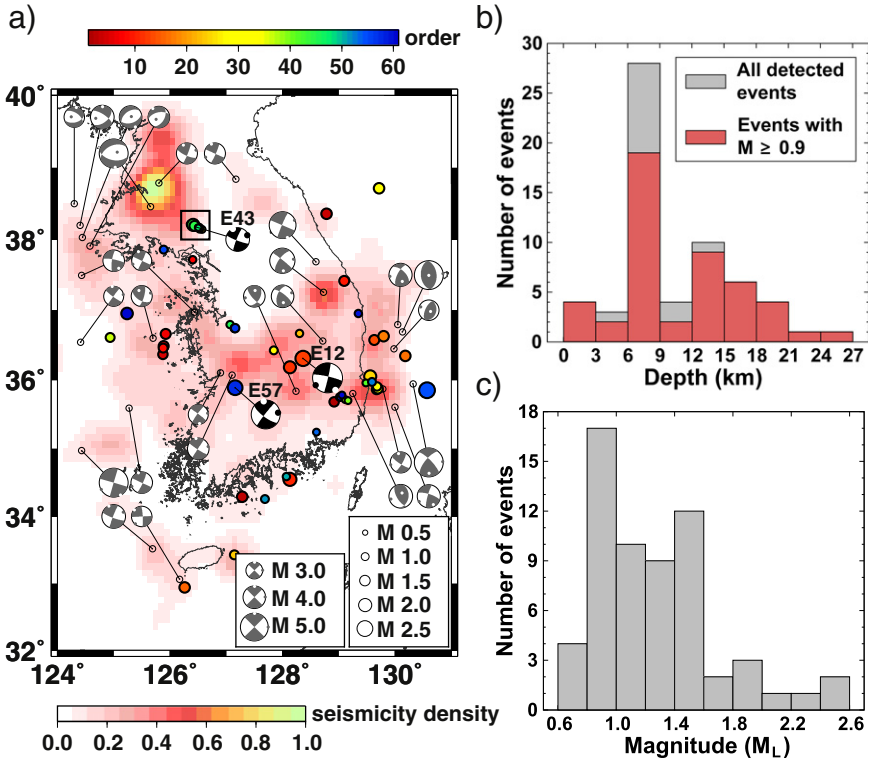

Fig. 6. (a) Spatial distribution of 61 identified events (filled circles) over the background seismicity density before the megathrust earthquake. The focal mechanism solutions of three detected events (E12, E43, E57) are presented in black. The focal mechanism solutions of events before the megathrust earthquake (gray) are presented for comparison. Earthquakes are clustered in a northwestern peninsula (boxed region). The detected events are generally distributed in regions of high seismicity density. Distribution of (b) focal depths and (c) magnitudes of detected events. The focal depths of events with magnitudes greater than or equal to 0.9 ensuring the complete event detection are presented in red.

We determine a set of parameters K, c and p maximizing the log-likelihood function using a grid search algorithm. An optimal K is searched between 1 and 30 with a discrete interval of 1, and an optimal c is searched between 0.1 and 3.0 h with a discrete interval of 0.02 h. Finally we test values for the optimal p between 0.5 and 2.0 in steps of 0.01 (Ogata, 1999). We also measure the eccentricity of seismicity in the given time period with respect to the background seismicity (Matthews and Reasenberg, 1988)

$$\beta = \frac{N_{obs} - \lambda t}{\sqrt{\lambda t}} \tag{10}$$

Table 1
Source information of earthquakes observed around the Korean Peninsula for 18 h following the 2011 M9.0 Tohoku-Oki earthquake. The hypocentral parameters of the earthquake swarm is further refined using a double difference location method. The horizontal and vertical location errors (e_h, e_z) and root-mean-squares traveltime errors (e_t) are presented.

ID	Date	Time (UTC)	Lat	Lon	Dep	Mag	e_h	e_z	e_t
	(yyyy/mm/dd)	(hh:mm:ss)	(°N)	(°E)	(km)	(M_L)	(km)	(km)	(s)
E01	2011/03/11	05:55:35.54	35.6840	128.9192	19.10	1.3	0.42	1.22	0.07
E02	2011/03/11	05:57:07.19	34.2927	127.2827	6.64	1.5	2.27	23.88	0.28
E03	2011/03/11	05:59:35.83	38.3608	128.7807	13.11	1.5	1.36	0.69	0.12
E04	2011/03/11	06:08:23.64	36.3643	125.8747	7.06	1.3	3.51	25.32	0.34
E05	2011/03/11	06:09:24.09	36.4863	125.8840	8.82	1.5	0.97	5.78	0.01
E06	2011/03/11	06:10:00.10	36.6617	125.9243	6.93	1.4	4.56	11.87	0.02
E07	2011/03/11	06:10:55.46	37.7158	126.4013	12.79	0.9	2.01	1.25	0.25
E08	2011/03/11	06:14:25.94	36.4575	125.8808	7.01	1.3	1.70	13.10	0.06
E09	2011/03/11	06:18:59.84	37.4148	129.0960	19.98	1.4	0.88	1.47	0.13
E10	2011/03/11	06:28:44.29	36.1803	128.1343	18.95	1.8	1.17	12.62	0.03
E11	2011/03/11	06:28:49.47	34.5460	128.1287	7.03	2.0	0.61	0.95	0.05
E12	2011/03/11	06:39:18.85	36.3065	128.3623	15.41	2.4	0.35	0.42	0.24
E13	2011/03/11	06:41:49.37	36.5725	129.6347	15.87	1.4	1.34	0.48	0.04
E14[a]	2011/03/11	06:42:11.28	38.178662	126.458521	6.079	0.9	0.05	0.04	0.02
E15	2011/03/11	06:43:46.18	32.9453	126.2605	6.79	1.5	1.62	18.10	0.21
E16	2011/03/11	07:40:03.69	36.3470	130.1837	23.12	1.5	3.38	1.48	0.10
E17	2011/03/11	07:47:37.04	36.6255	129.7950	14.08	1.5	1.03	0.70	0.11
E18	2011/03/11	08:48:06.36	35.7507	129.0228	18.38	1.0	12.76	1.67	0.04
E19[a]	2011/03/11	08:49:55.66	38.178394	126.457845	6.142	1.2	0.03	0.02	0.42
E20[a]	2011/03/11	08:58:06.66	38.177995	126.457438	6.184	1.0	0.03	0.04	0.08
E21[a]	2011/03/11	08:58:52.31	38.178162	126.458309	6.134	1.1	0.03	0.08	0.07
E22	2011/03/11	09:00:44.87	36.6653	128.3048	0.05	0.9	1.51	11.03	0.58
E23	2011/03/11	09:18:31.62	33.4307	127.1430	14.70	1.2	1.50	0.39	0.05
E24	2011/03/11	09:21:41.83	36.0495	129.5560	16.01	1.8	0.75	1.63	0.06
E25[a]	2011/03/11	09:23:55.59	38.1403	126.5717	6.93	0.8	0.12	0.08	0.30
E26	2011/03/11	09:45:16.63	35.8602	129.6700	7.04	1.3	1.64	12.44	0.03
E27	2011/03/11	10:00:14.99	36.4270	127.8465	13.13	1.0	12.64	0.04	0.03
E28[a]	2011/03/11	10:04:30.29	38.178992	126.455306	6.089	0.9	0.03	0.03	0.27
E29[a]	2011/03/11	10:11:04.77	38.178487	126.456641	6.043	1.5	0.02	0.02	0.20
E30	2011/03/11	10:12:39.14	35.8772	129.6913	7.04	1.4	2.26	12.46	0.08
E31[a]	2011/03/11	10:25:18.39	38.178520	126.456274	6.039	1.3	0.02	0.02	0.23
E32	2011/03/11	10:33:08.45	35.9018	129.6812	7.02	1.2	0.82	12.63	0.05
E33	2011/03/11	10:51:01.25	38.7173	129.7112	1.75	1.6	13.52	13.49	0.64
E34[a]	2011/03/11	10:54:37.10	38.1640	126.5108	6.77	0.7	0.12	0.08	0.15
E35[a]	2011/03/11	11:16:25.08	38.177600	126.457113	6.026	0.8	0.08	0.05	0.05
E36	2011/03/11	11:31:04.42	36.6105	124.9395	0.05	1.2	4.81	5.90	0.45
E37	2011/03/11	11:37:59.12	35.7143	129.1148	14.83	0.8	12.50	1.29	0.01
E38[a]	2011/03/11	11:48:12.19	38.1430	126.5253	5.58	0.8	0.12	0.08	0.27
E39	2011/03/11	13:10:31.98	35.6982	129.1602	12.70	0.9	12.53	1.04	0.01
E40[a]	2011/03/11	13:10:35.86	38.178475	126.456901	6.055	0.8	0.03	0.04	0.10
E41	2011/03/11	13:11:43.21	35.9575	129.4843	6.99	0.8	4.09	58.69	0.83
E42[a]	2011/03/11	13:12:50.44	38.177816	126.456258	6.012	0.7	0.12	0.08	0.00
E43[a]	2011/03/11	13:15:41.57	38.178792	126.455754	6.005	1.9	0.02	0.02	0.22
E44[a]	2011/03/11	13:55:07.30	38.178276	126.457137	6.033	1.4	0.02	0.02	0.21
E45	2011/03/11	14:03:21.80	36.7950	127.0677	10.13	0.9	0.77	4.24	0.28
E46[a]	2011/03/11	14:08:14.76	38.1705	126.4897	6.94	0.6	0.12	0.08	0.02
E47[a]	2011/03/11	14:15:40.80	38.178556	126.454867	5.989	0.8	0.03	0.03	0.04
E48	2011/03/11	14:18:41.72	36.7367	127.1517	15.44	0.9	0.59	0.62	0.14
E49	2011/03/11	14:20:30.13	36.7430	127.1472	11.93	1.0	0.76	1.63	0.12
E50	2011/03/11	14:29:32.84	34.5907	128.0708	26.65	0.9	1.86	2.07	0.07
E51	2011/03/11	14:45:50.69	34.2567	127.6845	7.00	1.1	1.46	15.50	0.14
E52	2011/03/11	15:50:26.31	35.9715	129.5925	15.53	1.1	1.06	0.74	0.16
E53	2011/03/11	16:39:56.66	35.2415	128.6020	6.64	0.8	5.49	9.33	0.06
E54	2011/03/11	17:29:38.74	35.8500	130.5648	12.11	2.5	4.55	5.03	0.37
E55	2011/03/11	17:40:46.35	37.8557	125.8877	5.24	1.0	0.71	5.23	0.15
E56	2011/03/11	20:06:49.89	36.7402	127.1598	12.09	1.1	0.47	1.12	0.18
E57	2011/03/11	20:26:54.83	35.8897	127.1532	17.79	2.3	0.31	0.56	0.17
E58	2011/03/11	20:33:09.93	35.7442	129.0220	11.85	0.7	12.58	1.72	0.02
E59	2011/03/11	22:44:27.04	36.9517	129.3475	14.01	1.0	0.79	0.94	0.09
E60	2011/03/11	23:15:35.27	36.9512	125.2357	0.03	1.7	2.09	5.25	0.31
E61	2011/03/11	23:21:38.17	35.7812	129.0548	11.07	0.8	0.74	2.01	0.08

[a] Earthquake swarm.

where N_{obs} is the observed number of earthquakes during the time duration t, and λ is the background earthquake occurrence rate.

5. Results

5.1. Dynamic stress changes

From Eq. (5), we calculate the dynamic stress change induced by seismic waves. We set the shear-wave velocity (V_s) and shear modulus (μ) to be 3.58 km/s and 34.95 GPa, respectively, considering the typical properties at a seismogenic depth (10 km) in the Korean Peninsula (Chang and Baag, 2006; Jo and Hong, 2013). The estimated peak dynamic strain (ε_m) varies from 1.12×10^{-6} to 12.84×10^{-6} (Fig. 4). The equivalent peak dynamic stress changes (σ_m) range from 0.039 to 0.449 MPa. The estimated dynamic stress changes are greater than the typical dynamic stress changes required for dynamic earthquake triggering (e.g., Hill and Prejean, 2007).

5.2. Event detection

We construct the reference traveltime matrix **M** using 70 vertical velocity seismograms (broadband and short-period waveforms) with high signal-to-noise ratios for earthquakes from 2001 to 2013. We calculate the waveform envelopes for signals bandpass-filtered between 5 and 20 Hz using a Hilbert transform (Earle and Shearer, 1994). We measure the STA/LTA amount based on the waveform envelopes. We set the waveform windows of STA and LTA to be 0.5 s and 5.0 s, respectively considering the typical frequency contents of seismic phases in local and regional distances (Trnkoczy, 2002). The STA/LTA estimates are stacked for all events by distance using the automatic gain control (AGC) algorithm (Shearer, 1991). We calculate the reference P and S traveltime curves using a linear regression of stacked STA/LTA, yielding apparent P and S velocities of 5.8 and 3.4 km/s, respectively (Fig. 5(a)).

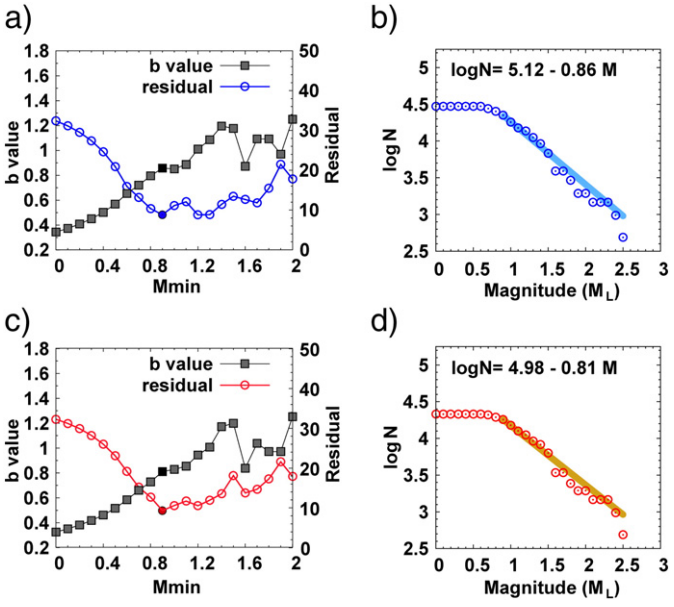

Fig. 7. (a) Variation of b values (filled squares) of triggered events as a function of minimum (cut-off) magnitude. The residuals (open circles) between the observed magnitudes and theoretical Gutenberg-Richter relationships present a minimum magnitude (M_{min}) of 0.9, the corresponding b value of which is 0.86. (b) Gutenberg-Richter magnitude-frequency relationship for triggered events. (c) Variation of b values (filled squares) and corresponding residuals for triggered events excluding the earthquake swarm. (d) Gutenberg-Richter magnitude-frequency relationship of events excluding the earthquake swarm. The b values are similar to those from all triggered events.

We analyze 20-h-long seismic records (2 h before and 18 h after the megathrust earthquake), and detect seismic events (Fig. 2). However, ambient noise may contaminate weak seismic signals. Thus, small seismic events in long distances may not be detected well. We divide the study region into 1.5° × 1.5° bins allowing overlapping of 1.0° with neighboring bins. Stations are grouped by location. We analyze the seismic waveforms of spatial bins with 5 or more stations. The number of resultant spatial bins analyzed is 75, which covers most areas of the southern peninsula and offshore regions (Fig. 5(b)).

We find 46,893 potential events from the 18-h-long record sections. Each potential event is examined for verification (Fig. 5(c)). No events are detected for 2 h before the megathrust earthquake. On the other hand, we observe 61 events for 18 h after the megathrust earthquake (Fig. 6). The hypocentral parameters of the verified events are refined using a conventional hypocentral-parameter inversion method based on the manually picked P and S arrival times (Klein, 2002). We apply a 1-D crustal velocity model of the Korean Peninsula model for the hypocentral-parameter inversion (Chang and Baag, 2006).

5.3. Seismic characterization

The detected events are clustered in the southeastern and western offshore regions and the southern peninsula, which are usual high-seismicity-density regions (Fig. 6). On the other hand, earthquakes are poorly detected in a high-seismicity-density region of North Korea between 38°N and 40°N and between 125°E and 126.5°E, which may be due to low detection capability in long distances (Fig. 1(b)). The magnitudes of detected events are M_L 0.5–2.5 (Table 1). Focal depths are clustered between 6 and 9 km and distributed up to 26.7 km (Fig. 6). In particular, micro-events with magnitudes less than 0.9 are observed at depths of 3–15 km.

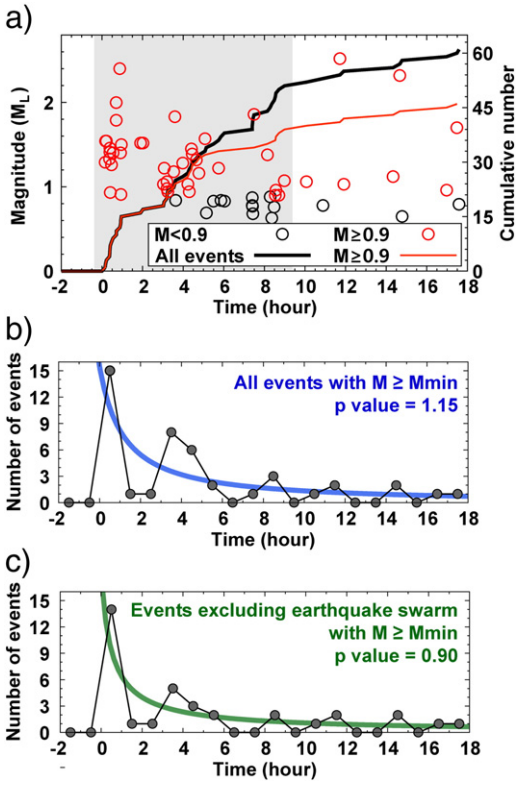

Fig. 8. (a) Cumulative numbers and magnitudes of earthquakes before and after the megathrust earthquake. No apparent correlations between magnitudes and lapse times are observed. (b) Number of earthquakes as a function of lapse time. The number of events decreases exponentially with lapse time, satisfying the modified Omori's law with a p value of 1.15. (b) Number of earthquakes as a function of time for events with magnitudes greater than or equal to M_{min} (=0.9). The p value is 0.90.

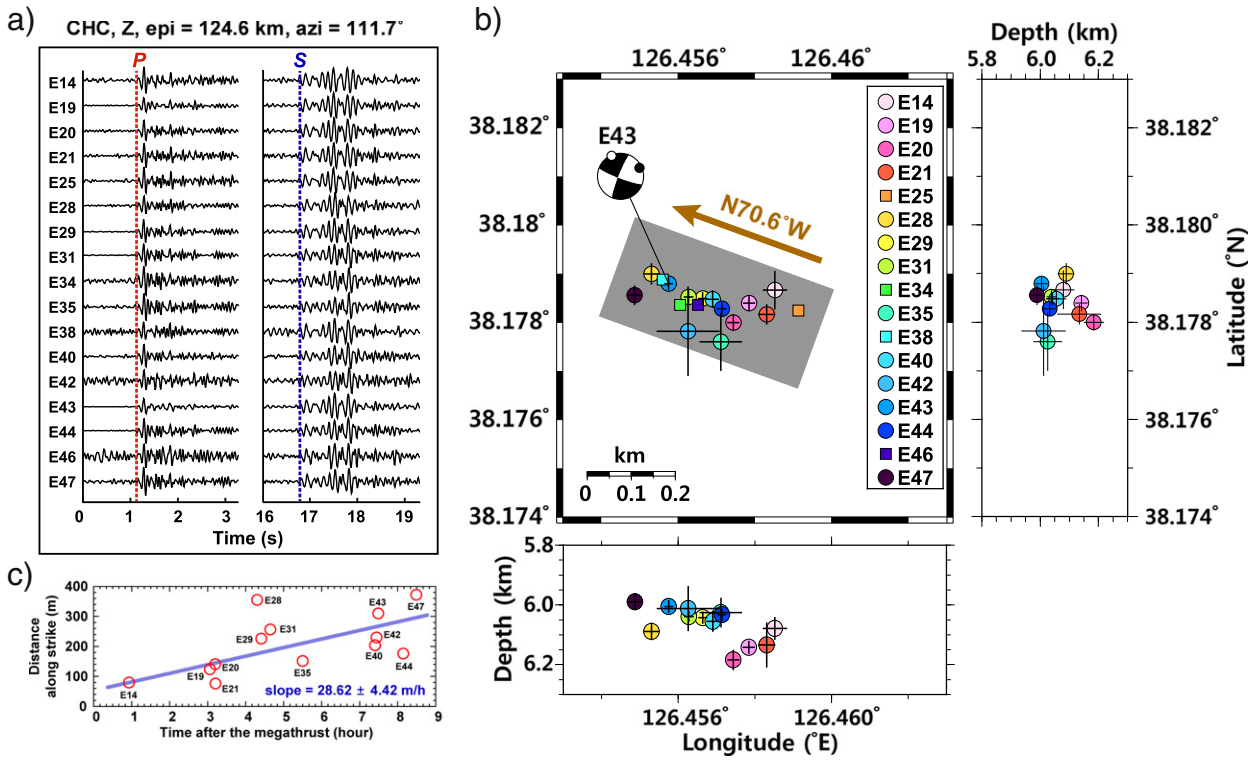

Fig. 9. (a) Vertical seismic waveforms of earthquake swarm recorded at station CHC in epicentral distances of ~124.6 km. The waveforms are similar to each other. (b) Epicenters and focal depths of earthquake swarm. The location errors are presented with solid bars. The focal mechanism solution of event E43 is consistent with the spatial distribution of events. The events are clustered at depths of ~6.1 km. The events migrate along N70.6 °W. (c) Temporal migration of earthquakes. The migration speed is determined to be 28.6 ± 4.4 m/h.

We determine the minimum magnitude (M_{min}) ensuring the complete observation of triggered events. The minimum magnitude of catalog is determined by a residual analysis of observed magnitudes of events with respect to the theoretical Gutenberg-Richter magnitude-frequency curve (Wiemer and Wyss, 2000; Houng and Hong, 2013; Hong et al., 2016). We find the minimum magnitude (M_{min}) of the observed triggered events to be 0.9 (Fig. 7). The number of events with magnitudes greater than or equal to M_{min} is 46. We identify one event at the time of surface-wave arrival. The other events are observed after the passage of surface waves. We find 15 events (33%) in the first hour after the megathrust earthquake and 17 events (37%) in the following 4 h (Fig. 8). The number of events exponentially decreases with time, satisfying the modified Omori's law. We found the parameter p in Eq. (7) to be 1.15. The parameters K and c are found to be 22 and 1.36 h, respectively (Fig. 8). On the other hand, parameters p, K and c are found to be 0.90, 9, and 0.46 h for triggered earthquakes excluding earthquake swarm. The estimated p values agree with those (~1.0) observed in near-field aftershocks (Shcherbakov et al., 2013). The agreement with the modified Omori law suggests the observed events are dynamically triggered earthquakes (e.g., Parsons, 2005).

We found the constants of the Gutenberg-Richter magnitude-frequency relationship to be $a = 5.12$ and $b = 0.86$, while $a = 5.01$ and $b = 0.84$ for events excluding the earthquake swarm. The observed b values are comparable to the b value (=0.81) of the background seismicity before the megathrust earthquake (Houng and Hong, 2013). On the other hand, the a values are greatly increased after the

Table 2
Comparison of properties of dynamically triggered earthquakes among various environments.

ID	Type[a]	Site[b]	Epicenter[c]	Date	Mainshock magnitude	Distance (km)	Background seismicity		Triggered seismicity						Ref.[g]
							Rate	M_{min}	Rate	M_{min}	M_{max}	p[d]	b[e]	Calib. rate[f]	
a1	GE	TG	Landers	1992/06/28	M_w 7.3	763	45/24 h	M_c 0.2	52/4 h	M_c 0.2	–	0.9	2.0	3/18 h	ST
a2	GE	Yell	Denali	2002/11/03	M_w 7.9	3100	0.7/24 h	M_c 1.5	250/24 h	M_c 1.5	M_c 3.2	1.02	2.0	3719/18 h	HU
b1	PB	ITVC	Nicoya	2012/09/05	M_w 7.6	200	5.5/24 h	M_c 0.5	300/24 h	M_c 0.5	M_c 3.5	1.017	0.7	141/18 h	LU
b2	PB	CSA	Dusky S.	2009/07/15	M_w 7.8	350	1000/1 y	M_L 1.0	51/24 h	M_L 1.0	–	1.0	0.7	51/18 h	BO
c1	AI	Yunnan	Sumatra	2004/12/26	M_w 9.1	2700	4500/1 y	M_L 1.5	800/14d	M_L 1.5	M_L 5.1	1.33	0.82	1607/18 h	LU
c2	AI	Utah	Denali	2002/11/03	M_w 7.9	3350	337/1073 d	M_L 1.5	7/24 h	M_L 1.5	–	0.53	0.6	14/18 h	PA
d1	SI	KP	Tohoku	2011/03/11	M_w 9.0	1300	355/16 y	M_L 2.5	61/18 h	M_L 0.9	M_L 2.5	1.15	0.8	61/18 h	TS

[a] Type of site: GE (geothermal area), PB (plate boundary), AI (active intraplate region), SI (stable intraplate region).
[b] TG (The Geysers, California, U.S.), Yell (Yellowstone, Wyoming, U.S.), ITVC (Irazú-Turrialba volcanic complex, Costa Rica), CSA (central Southern Alps, South Island, New Zealand), Yunan (Yunnan, southwestern China), KP (Korean Peninsula).
[c] Epicenter location: Landers (Landers earthquake), Denali (Denali fault earthquake), Nicoya (Nicoya earthquake), Dusky S. (Dusky Sound earthquake), Sumatra (Sumatra-Andaman earthquake), Tohoku (Tohoku-Oki earthquake).
[d] P value in the modified Omori law.
[e] b (b value in the Gutenberg-Richter frequency-magnitude relationship). Some b values are collected from other studies (Murru et al., 1999; Ghosh et al., 2008; Hong et al., 2015).
[f] Calibrated occurrence rate of triggered earthquakes with magnitudes greater than or equal to $M_{min} = 0.9$ for 18 h.
[g] References: ST (Stark and Davis, 1996), HU (Husen et al., 2004), LU (Lupi et al., 2014), BO (Boese et al., 2014), PA (Pankow et al., 2004), TS (this study) magnitude symbols: M_w (moment magnitude), M_c (coda magnitude), M_L (local magnitude), M_{min} (minimum magnitude ensuring the completeness of earthquake catalog), M_{max} (observed maximum magnitude).

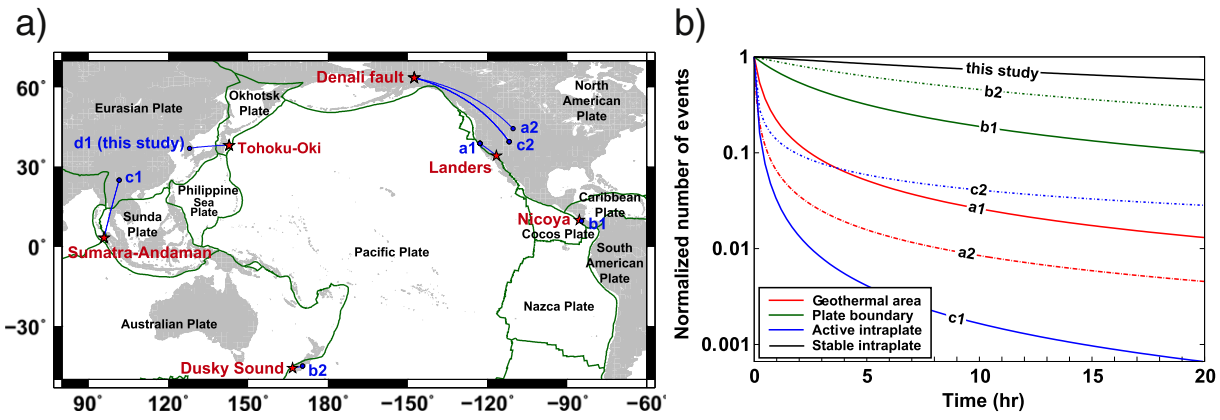

Fig. 10. (a) Map of locations of dynamic triggering (circles) and mainshocks (stars). The great-circle paths are marked with solid lines. Areas of dynamic triggering include geothermal regions (the Geysers (a1), Yellowstone (a2)), plate boundary regions (Irazú volcanic complex, Costa Rica (b1), central southern Alps, New Zealand (b2)), active intraplate regions (Yunan, China (c1), Utah, US (c2)), and a stable intraplate region (Korean Peninsula (d1)). (b) Normalized number of earthquakes as a function of lapse time. The triggered earthquakes from the stable intraplate region (d1) display the lowest temporal decay rate, while geothermal regions (a1, a2) and active intraplate regions (c1, c2) present high decay rates.

megathrust earthquake ($a = 3.33$ in background seismicity before the megathrust earthquake). We find parameter β to be 49.9 for events with $M \geq 0.9$. The observation indicates a large increase of seismicity holding the relative magnitude-dependent occurrence frequency. This feature suggests that the seismicity was increased as a consequence of medium response to the dynamic stress changes induced by strong seismic waves from the megathrust earthquake (e.g., Gomberg et al., 1998).

We determine the focal mechanism solutions of two events with good azimuthal coverage (events E12 and E54) using seismic-polarity analysis (Fig. 6) (Hardebeck and Shearer, 2002, 2003). The focal mechanism solutions are similar to those observed before the megathrust earthquake (Choi et al., 2012; Hong and Choi, 2012). This feature results from the coincidence of the responsible compression-axis direction with the ambient stress field before the megathrust earthquake. The characteristic geometry of the Korean Peninsula with respect to the epicenter of the megathrust earthquake constructs a transient stress field that is subparallel to the ambient stress field (Fig. 1).

5.4. Earthquake swarm

We identify an earthquake swarm composed of 17 earthquakes in a region of 350 m by 160 m area around 38.2°N and 126.5°E. The earthquake swarm occurred 56 min after the megathrust earthquake, lasting for 454 min (Table 1). The waveforms are highly similar among the events of earthquake swarm, suggesting occurrence on the same fault zone (Fig. 9). The hypocenters of 13 events are refined using a double difference location algorithm (Waldhauser and Ellsworth, 2000) (Table 1). The other 4 events are relocated with respect to the 13 events by using the traveltime differences between *P* and *S* waves. The traveltime differences are measured using a waveform cross-correlation.

The focal depths of the earthquake swarm range between 6.0 and 6.2 km. The spatial distribution of events resembles a near-vertical fault plane striking in ESE-WNW, which is consistent with the strike of fault plane of event E43 (292°) (Fig. 6). We find that the earthquake swarm migrated along N70.6°W with a speed of 28.6 ± 4.4 m/h (Fig. 9). The migration direction is consistent with the fault strike. The migration speed is similar to those observed from the induced seismicity in fluid injection sites (20–80 m/h; Tadokoro et al., 2000). This observation suggests that the earthquake swarm might be triggered by transient pore-fluid pressure change due to seismic waves from the megathrust earthquake.

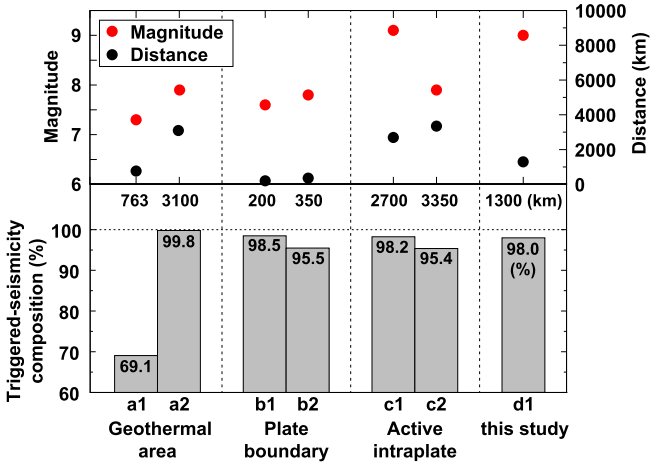

Fig. 11. Composition amounts of triggered earthquakes among all observed earthquakes for 36 h (18 h before and 18 h after the mainshocks) for various tectonic environments. The magnitudes of mainshocks and the epicentral distances are denoted on the upper panel, and the composition of triggered earthquakes are presented with histograms in the lower panel. The compositions of triggered seismicity make up more than 69% in all environments including the Korean Peninsula, which is considered this study.

6. Properties of dynamic triggering

It is known that earthquake triggering by dynamic stress change preferentially occurs in active faults or geothermal areas (e.g., Hough et al., 2003; Peng et al., 2010; Jiang et al., 2010). We compare the properties of the dynamic triggering around the Korean Peninsula with those in other environments including geothermal, active plate boundary, and active intraplate regions (Table 2). The regions are Yellowstone and the Geysers as geothermal areas (Stark and Davis, 1996; Husen et al., 2004), the central southern Alps in New Zealand and Irazú volcanic complex, Costa Rica as plate boundary areas (Lupi et al., 2014; Boese et al., 2014), and Yunan, China and Utah, US as active intraplate areas (Pankow et al., 2004; Lupi et al., 2014). The Korean Peninsula is a stable intraplate region (Fig. 10).

The earthquakes responsible for the dynamic triggering include the 3 November 2002 M_w7.9 Denali earthquake, 28 June 1992 M_w7.3 Landers earthquake, 5 September 2012 M_w7.6 Nicoya earthquake, 15 July 2009 M_w7.8 Dusky Sound earthquake, 26 December 2004 M_w9.1 Sumatra-Andaman earthquake, and 11 March 2011 M_w9.0 Tohoku-Oki earthquake (Fig. 10(a)). The epicentral distances vary between 200 and 3350 km. The observed periods of triggered seismicity and the minimum magnitudes are not uniform among the studies (Table 2). The occurrence rates of triggered earthquakes are calibrated for a duration of 18 h and minimum magnitude (M_{min}) of 0.9. The background

seismicity rates and the minimum magnitudes are presented for reference.

The triggered-earthquake occurrence rate might be dependent on the magnitude and distance. Further, the triggered-earthquake occurrence rate generally decays with time. The triggered earthquakes decay fast in geothermal and active intraplate regions (Fig. 10(b)). On the other hand, the decay rates of triggered-earthquake occurrence are relatively slow in plate boundary regions compared to those in other active regions. It is intriguing to note that the decay rate of triggered earthquakes is slowest in the Korean Peninsula. The total numbers of triggered earthquakes may be large in active seismic regions such as geothermal, plate-boundary, and active intraplate regions. However, the normalized duration of dynamic triggering is large in the stable intraplate region. Further, the decay rates of triggered-earthquake occurrence suggest long-time dominance of triggered earthquakes in stable intraplate and plate boundary regions. This observation suggests that the ambient stress level of a stable intraplate region may be close to the critical level of faulting caused by long-term lithostatic loading. The abrupt addition of transient stress may yield the dynamic triggering of earthquakes in such stable intraplate regions.

Fig. 11 presents the composition amounts of triggered earthquakes among all observed earthquakes for 36 h (18 h before and 18 h after the mainshocks) in various tectonic environments. The triggered earthquakes make up more than 95% in most regions except the Geysers (a1). This observation suggests that dynamic triggering can be dominant in any type of region. Moreover, the strength of dynamic triggering may be a consequence of composite effects of mainshock magnitude and distance. However, the Gutenberg-Richter *b* values and largest magnitudes of triggered earthquakes are significantly different among different regions (Table 2). The *b* values are generally high in the geothermal regions, while they are relatively low in the stable intraplate region. This observation suggests that magnitude-dependent earthquake occurrence frequency and triggered-earthquake sizes might be dependent on the medium properties. Further, the dynamically triggered earthquakes can occur in any type of regions.

7. Discussion and conclusions

We investigated the dynamic triggering of earthquakes around the Korean Peninsula by the 2011 M9.0 Tohoku-Oki earthquake. Strong seismic waves from the megathrust earthquake accompany dynamic stress changes of 0.039–0.449 MPa around the Korean Peninsula, triggering 61 earthquakes including an earthquake swarm composed of 17 events for 18 h following the megathrust earthquake. The triggered earthquakes are distributed in regions of high background seismicity. Further, the earthquake swarm appears to have migrated along N70.6°W with a speed of 28.6 ± 4.4 m/h, suggesting the influence of pore-fluid pressure on the triggering of earthquakes.

The occurrence of triggered earthquakes decreases with time following the modified Omori law with a *p* value of 1.15. The occurrence of triggered earthquakes caused the Gutenberg-Richter *a* value to increase after the megathrust earthquake. We, however, found that the Gutenberg-Richter *b* value is invariant. Also, we observed that focal mechanism solutions are nearly consistent with those before the megathrust earthquake. The dynamic triggering can occur in any types of sites (Velasco et al., 2008). However, the strength of the dynamic triggering may be dependent on the mainshock magnitude and distance. Also, the triggered earthquakes of the stable intraplate region appear to occur in locations with long-term loading lithostatic stress close to the critical stress level of faulting.

Acknowledgements

We are grateful to anonymous reviewers for constructive review comments that improved the presentation of the manuscript. We thank Dr. Taka'aki Taira from Berkeley Seismological Laboratory for valuable comments on dynamic stress change. We are grateful to the Korea Meteorological Administration (KMA) and Korea Institute of Geoscience and Mineral Resources (KIGAM) for making seismic waveforms available. This work was supported by the Korea Meteorological Administration Research and Development Program under Grant KMIPA 2015-7040. Also, this research was partly supported by the Basic Science Research Program through the National Research Foundation of Korea (NRF) funded by the Ministry of Education (2015R1D1A1A01060198).

References

Asano, Y., Saito, T., Ito, Y., Shiomi, K., Hirose, H., Matsumoto, T., Aoi, S., Hori, S., Sekiguchi, S., 2011. Spatial distribution and focal mechanisms of aftershocks of the 2011 off the Pacific coast of Tohoku earthquake. Earth Planets Space 63, 669–673.

Atkinson, B.K., 1984. Subcritical crack growth in geologic materials. J. Geophys. Res. 89, 4077–4114.

Baek, J., Shin, Y.-H., Na, S.-H., Shestakov, N.V., Park, P.-H., Cho, S., 2012. Coseismic and postseismic crustal deformations of the Korean Peninsula caused by the 2011 Mw 9.0 Tohoku earthquake, Japan, from global positioning system data. Terra Nova 24, 295–300.

Boese, C.M., Jacobs, K.M., Smith, E.G.C., Stern, T.A., Townend, J., 2014. Background and delayed-triggered swarms in the central Southern Alps, South Island, New Zealand. Geochem. Geophys. Geosyst. 15, 945–964.

Bohnenstiehl, D.R., Tolstoy, M., Dziak, R.P., Fox, C.G., Smith, D.K., 2002. Aftershock sequences in the mid-ocean ridge environment: an analysis using hydroacoustic data. Tectonophysics 354, 49–70.

Brodsky, E.E., Karakostas, V., Kanamori, H., 2000. A new observation of dynamically triggered regional seismicity: earthquakes in Greece following the August 1999 Izmit, Turkey earthquake. Geophys. Res. Lett. 27, 2741–2744.

Brodsky, E.E., Roeloffs, E., Woodcock, D., Gall, I., Manga, M., 2003. A mechanism for sustained groundwater pressure changes induced by distant earthquakes. J. Geophys. Res. 108, 2390. http://dx.doi.org/10.1029/2002JB002321.

Chang, S.-J., Baag, C.-E., 2006. Crustal structure in southern Korea from joint analysis of regional broadband waveforms and travel times. Bull. Seismol. Soc. Am. 96, 856–870.

Chen, W.P., Molnar, P., 1983. Focal depths of intracontinental and intraplate earthquakes and their implications for the thermal and mechanical properties of the lithosphere. J. Geophys. Res. 88, 4183–4214.

Choi, H.I., 1986. Sedimentation and evolution of the Cretaceous Gyeongsang Basin, southeastern Korea. J. Geol. Soc. 143, 29–40.

Choi, H., Hong, T.-K., He, X., Baag, C.-E., 2012. Seismic evidence for reverse activation of a paleo-rifting system in the East Sea (Sea of Japan). Tectonophysics 572-573, 123–133.

Choi, J., Kang, T.S., Baag, C.-E., 2009. Three-dimensional surface wave tomography for the upper crustal velocity structure of southern Korea using seismic noise correlations. Geosci. J. 13, 423–432.

Chough, S.K., Kwon, S.-T., Ree, J.-H., Choi, D.K., 2000. Tectonic and sedimentary evolution of the Korean peninsula: a review and new view. Earth Sci. Rev. 52, 175–235.

Earle, P., Shearer, P.M., 1994. Characterization of global seismograms using an automatic-picking algorithm. Bull. Seismol. Soc. Am. 84, 276–366.

Engdahl, E.R., Villasenor, A., 2002. Global Seismicity: 1900–1999. In: Lee, W.H.K., Kanamori, H., Jenning, P.C., Kisslinger, C. (Eds.), International Handbook of Earthquake and Engineering Seismology, Part A Chapter 41. Academic Press, New York, pp. 665–690.

Ernst, W.G., Tsujimori, T., Zhang, R., Liou, J.G., 2007. Permo-Triassic collision, subduction-zone metamorphism, and tectonic exhumation along the east Asian continental margin. Annu. Rev. Earth Planet. Sci. 35, 73–110.

Freed, A.M., Lin, J., 2001. Delayed triggering of the 1999 Hector Mine earthquake by viscoelastic stress transfer. Nature 411, 180–183.

Freed, A.M., 2005. Earthquake triggering by static, dynamic, and postseismic stress transfer. Annu. Rev. Earth Planet. Sci. 33, 335–367.

Ghosh, A., Newman, A.V., Thomas, A.M., Farmer, G.T., 2008. Interface locking along the subduction megathrust from b-value mapping near Nicoya Peninsula, Costa Rica. Geophys. Res. Lett. 35, L01301. http://dx.doi.org/10.1029/2007GL031617.

Gomberg, J., Beeler, N.M., Blanpied, M.L., Bodin, P., 1998. Earthquake triggering by transient and static deformations. J. Geophys. Res. 103, 24411–24426.

Gomberg, J., Bodin, P., Larson, K., Dragert, H., 2004. Earthquake nucleation by transient deformations caused by the M = 7.9 Denali, Alaska, earthquake. Nature 427, 621–624.

Gonzalez-Huizar, H., Velasco, A.A., 2011. Dynamic triggering: stress modeling and a case study. J. Geophys. Res. 116, B02304. http://dx.doi.org/10.1029/2009JB007000.

Gonzalez-Huizar, H., Velasco, A.A., Peng, A., Castro, R.R., 2012. Remote triggered seismicity caused by the 2011, M9.0 Tohoku-Oki, Japan earthquake. Geophys. Res. Lett. 39, L10302. http://dx.doi.org/10.1029/2012GL051015.

Hardebeck, J.L., Shearer, P.M., 2002. A new method for determining first motion focal mechanisms. Bull. Seismol. Soc. Am. 92, 2264–2276.

Hardebeck, J.L., Shearer, P.M., 2003. Using S/P amplitude ratios to constrain the focal mechanisms of small earthquakes. Bull. Seismol. Soc. Am. 93, 2434–2444.

Hill, D.P., Reasenberg, P.A., Michael, A., Arabaz, W.J., Beroza, G., Brumbaugh, D., Brune, J.N., Castro, R., Davis, S., dePolo, D., Ellsworth, W.L., Gomberg, J., Harmsen, S., House, L., Jackson, S.M., Johnston, M.J.S., Jones, L., Keller, R., Malone, S., Munguia, L., Nava, S., Pechmann, J.C., Sanford, A., Simpson, R.W., Smith, R.B., Stark, M., Stickney, M., Vida, A., Walter, S., Wong, V., J., Z., 1993. Seismicity remotely triggered by the magnitude 7.3 landers, California, earthquake. Science 260, 1617–1623.

Hill, D.P., Prejean, S.G., 2007. Dynamic Triggering. In: Kanamori, H. (Ed.), Earthquake Seismology, Treatise on Geophysics Vol. volume 4. Elsevier, Amsterdam, pp. p257–p291.
Hirata, N., Tokuyama, H., Chung, T.W., 1989. An anomalously thick layering of the crust of the Yamato basin, southeastern sea of Japan: the final stage of back-arc spreading. Tectonophysics 165, 303–314.
Hong, T.-K., 2010. Lg attenuation in a region with both continental and oceanic environments. Bull. Seismol. Soc. Am. 100, 851–858.
Hong, T.-K., Baag, C.-E., Choi, H., Sheen, D.-H., 2008. Regional seismic observations of the 9 October 2006 underground nuclear explosion in North Korea and the influence of crustal structure on regional phases. J. Geophys. Res. 113, B03305. http://dx.doi.org/10.1029/2007JB004950.
Hong, T.-K., Baag, C.-E., Shin, J.S., 2000. The M_L scale in southern Korea. J. Geol. Soc. Korea 36, 545–558 (in Korean).
Hong, T.-K., Choi, H., 2012. Seismological constraints on the collision belt between the North and South China blocks in the Yellow Sea. Tectonophysics 570-571, 102–113.
Hong, T.-K., Kang, T.-S., 2009. Pn travel-time tomography of the paleo-continental-collision and rifting zone around Korea and Japan. Bull. Seismol. Soc. Am. 99, 416–421.
Hong, T.-K., Lee, J., Houng, S.E., 2015. Long-term evolution of intraplate seismicity in stress shadows after a megathrust. Phys. Earth Planet. Inter. 245, 59–70.
Hong, T.-K., Park, S., Houng, S.E., 2016. Seismotectonic properties and zonation of the far-eastern Eurasian plate around the Korean Peninsula. Pure Appl. Geophys. 173 (4), 1175–1195.
Hoshiba, M., Iwakiri, K., Hayashimoto, N., Shimoyama, T., Hirano, K., Yamada, Y., Ishigaki, Y., Kikuta, H., 2011. Outline of the 2011 off the Pacific coast of Tohoku earthquake (Mw 9.0)-earthquake early warning and observed seismic intensity. Earth Planets Space 63, 547–551.
Hough, S.E., 2001. Triggered earthquakes and the 1811-1812 New Madrid, Central United States, earthquake sequence. Bull. Seismol. Soc. Am. 91, 1574–1581.
Hough, S.E., Seeber, L., Armbruster, J.G., 2003. Intraplate triggered earthquakes: observations and interpretation. Bull. Seismol. Soc. Am. 93, 2212–2221.
Houng, S.E., Hong, T.-K., 2013. Probabilistic analysis of the Korean historical earthquake records. Bull. Seismol. Soc. Am. 103, 2782–2796.
Husen, S., Wiemer, S., Smith, R.B., 2004. Remotely triggered seismicity in the Yellowstone National Park Region by the 2002 Mw 7.9 Denali Fault earthquake, Alaska. Bull. Seismol. Soc. Am. 94, S317–S331.
Irikura, K., Kurahashi., S., 2012. Strong Ground Motions during the 2011 Pacific Coast off Tohoku, Japan Earthquake. International Symposium on Engineering Lessons Learned from the Giant Earthquake, March 1–4, Tokyo, Japan.
Jiang, T., Peng, Z., Wang, W., Chen, Q.F., 2010. Remotely triggered seismicity in continental China following the 2008 Mw 7.9 Wenchuan earthquake. Bull. Seismol. Soc. Am. 100, 2574–2589.
Jo, E., Hong, T.-K., 2013. Vp/Vs ratios in the upper crust of the southern Korean Peninsula and their correlations with seismic and geophysical properties. J. Asian Earth Sci. 66, 204–214.
Johnson, P.A., Jia, X., 2005. Nonlinear dynamics, granular media and dynamic earthquake triggering. Nature 437, 871–874.
Jolivet, L., Tamaki, K., Fournier, M., 1994. Japan Sea, opening history and mechanism: a synthesis. J. Geophys. Res. 99, 22237–22259.
Kang, T.S., Shin, J.S., 2006. Surface-wave tomography from ambient seismic noise of accelerograph networks in southern Korea. Geophys. Res. Lett. 33, L17303. http://dx.doi.org/10.1029/2006GL027044.
Kilb, D., Gomberg, J., Bodin, P., 2002. Aftershock triggering by complete Coulomb stress changes. J. Geophys. Res. 107, ESE-2. http://dx.doi.org/10.1029/2001JB000202.
Kim, H.-J., Han, S.-J., Lee, G.H., Huh, S., 1998. Seismic study of the Ulleung Basin crust and its implications for the opening of the East Sea (Japan Sea). Mar. Geophys. Res. 20, 219–237.
Kim, S.K., Park, M.A., 2005. The local magnitude scale in the Korean Peninsula. Pure Appl. Geophys. 162, 875–889.
Kim, S.-K., Bae, T.-S., 2012. Analysis of crustal deformation on the Korea Peninsula after the 2011 Tohoku earthquake. J. Korean Soc. Surv. Geod. Photogram. Cartograp. 30, 87–96.
King, G.C., Stein, R.S., Lin, J., 1994. Static stress changes and the triggering of earthquakes. Bull. Seismol. Soc. Am. 84, 935–953.
Klein, F.W., 2002. User's Guide to HYPOINVERSE-2000: A Fortran Program to Solve for Earthquake Locations and Magnitudes. U.S. Geological Survey, pp. 1–123.
Knopoff, L., Gardner, J.K., 1972. Higher seismic activity during local night on the raw worldwide earthquake catalog. Geophys. J. Int. 28, 311–313.
Kulinich, R.G., Valitov, M.G., 2011. Thicknesses and types of the crust beneath the Sea of Japan inferred from marine and satellite gravimetric investigations. Russ. J.Pacific Geol. 5, 481–491.
Lay, T., Ammon, C.J., Kanamori, H., Xue, L., Kim, M.J., 2011. Possible large near-trench slip during the 2011 Mw 9.0 off the Pacific coast of Tohoku earthquake. Earth Plan. Space 63, 687–692.
Lee, H.A., Woo, N.C., 2012. Influence of the M 9.0 Tohoku earthquake on groundwater in Korea. Geosci. J. 16, 1–6.
Lee, S.H., Ha, K., Shin, J.S., Ko, K.S., Hamm, S.Y., 2013. Successive groundwater level changes on Jeju Island due to the Mw 9.0 off the Pacific coast of Tohoku earthquake. Bull. Seismol. Soc. Am. 103, 1614–1621.
Lee, J., Hong, T.-K., 2014. Dynamic lithospheric response to megathrust and precursory seismicity features of megathrust. Phys. Earth Planet. Inter. 245, 59–70.
Lupi, M., Fuchs, F., Pacheco, J.F., 2014. Fault reactivation due to the M7.6 Nicoya earthquake at the Turrialba-Irazú volcanic complex, Costa Rica: effects of dynamic stress triggering. Geophys. Res. Lett. 41, 4142–4148.
Matthews, M.V., Reasenberg, P.A., 1988. Statistical methods for investigating quiescence and other temporal seismicity patterns. Pure Appl. Geophys. 126, 357–372.
Miyazawa, M., Mori, J., 2005. Detection of triggered deep low-frequency events from the 2003 Tokachi-oki earthquake. Geophys. Res. Lett. 32, L10307. http://dx.doi.org/10.1029/2005GL022539.
Miyazawa, M., 2011. Propagation of an earthquake triggering front from the 2011 Tohoku-Oki earthquake. Geophys. Res. Lett. 38, L23307. http://dx.doi.org/10.1029/2011GL049795.
Mori, N., Takahashi, T., Yasuda, T., Yanagisawa, H., 2011. Survey of 2011 Tohoku earthquake tsunami inundation and run-up. Geophys. Res. Lett. 38, L00G14. http://dx.doi.org/10.1029/2011GL049210.
Murru, M., Montuori, C., Wyss, M., Privitera, E., 1999. The locations of magma chambers at Mt. Etna, Italy, mapped by b-values. Geophys. Res. Lett. 26 (16), 2553–2556.
Ogata, Y., 1999. Seismicity analysis through point-process modeling: a review. Pure Appl. Geophys. 155, 471–507.
Oh, C.W., 2006. A new concept on tectonic correlation between Korea, China, and Japan: histories from the late Proterozoic to Cretaceous. Gondwana Res. 9, 47–61.
Pankow, K.L., Arabasz, W.J., Pechmann, J.C., Nava, S.J., 2004. Triggered seismicity in Utah from the 3 November 2002 Denali fault earthquake. Bull. Seismol. Soc. Am. 94, S332–S347.
Parsons, T., 2005. A hypothesis for delayed dynamic earthquake triggering. Geophys. Res. Lett. 32, L04302. http://dx.doi.org/10.1029/2004GL021811.
Parsons, T., Ji, C., Kirby, E., 2008. Stress changes from the 2008 Wenchuan eartccchquake and increased hazard in the Sichuan basin. Nature 454, 509–510.
Parsons, T., Velasco, A.A., 2011. Absence of remotely triggered large earthquakes beyond the mainshock region. Nat. Geosci. 4 (5), 312–316.
Pasyanos, M.E., Franz, G.A., Ramirez, A.L., 2006. Reconciling a geophysical model to data using a Markov chain Monte Carlo algorithm: an application to the Yellow Sea-Korean Peninsula region. J. Geophys. Res. 111, B03313. http://dx.doi.org/10.1029/2005JB003851.
Peng, Z., Wang, W., Chen, Q.F., Jiang, T., 2010. Remotely triggered seismicity in North China following the 2008 Mw 7.9 Wenchuan earthquake. Earth Planets Space 62, 893–898.
Peng, Z., Aiken, C., Kilb, D., Shelly, D.R., Enescu, B., 2012. Listening to the 2011 magnitude 9.0 Tohoku-Oki, Japan, earthquake. Seismol. Res. Lett. 83, 287–293.
Reasenberg, P.A., Simpson, R.W., 1992. Response of regional seismicity to the static stress change produced by the Loma Prieta earthquake. Science 255, 1687–1690.
Saccorotti, G., Piccinini, D., Mazzarini, F., Zupo, M., 2013. Remotely triggered micro-earthquakes in the Larderello-Travale geothermal field (Italy) following the 2012 May 20, Mw 5.9 Po-plain earthquake. Geophys. Res. Lett. 40, 835–840.
Sato, T., Sato, T., Shinohara, M., Hino, R., Nishino, M., Kanazawa, T., 2006. P-wave velocity structure of the margin of the southeastern Tsushima basin in the Japan Sea using ocean bottom seismometers and airguns. Tectonophysics 3-4, 159–171.
Shcherbakov, R., Goda, K., Ivanian, A., Atkinson, G.M., 2013. Aftershock statistics of major subduction earthquakes. Bull. Seismol. Soc. Am. 103, 3222–3234.
Shearer, P.M., 1991. Imaging global body wave phases by stacking long-period seismograms. J. Geophys. Res. 96 (B12), 20353–20364.
Stark, S.D., Davis, S.D., 1996. Remotely triggered microearthquakes at the Geysers geothermal field, California. Geophys. Res. Lett. 23, 945–948.
Stein, R.S., 1999. The role of stress transfer in earthquake occurrence. Nature 402, 605–609.
Stein, R.S., King, G.C., Lin, J., 1992. Change in failure stress on the southern San Andreas fault system caused by the 1992 magnitude = 7.4 landers earthquake. Science 258, 1328–1332.
Tadokoro, K., Ando, M., Nishigami, K.Y., 2000. Induced earthquakes accompanying the water injection experiment at the Nojima fault zone, Japan: seismicity and its migration. J. Geophys. Res. 105, 6089–6104.
Tajima, F., Mori, J., Kennett, B.L.N., 2013. A review of the 2011 Tohoku-Oki earthquake (Mw 9.0): large-scale rupture across heterogeneous plate coupling. Tectonophysics 586, 15–34.
Takahashi, H., 2011. Static strain and stress changes in eastern Japan due to the 2011 off the Pacific coast of Tohoku earthquake, as derived from GPS data. Earth Planets Space 63, 741–744.
Tibi, R., Wiens, D.A., Inoue, H., 2003. Remote triggering of deep earthquakes in the 2002 Tonga sequences. Nature 424, 921–925.
Tinti, S., Mulargia, F., 1987. Confidence intervals of b values for grouped magnitudes. Bull. Seismol. Soc. Am. 77, 2125–2134.
Toda, S., Lin, J., Stein, R.S., 2011. Using the 2011 Mw 9.0 off the Pacific coast of Tohoku earthquake to test the Coulomb stress triggering hypothesis and to calculate faults brought closer to failure. Earth Planets Space 63, 725–730.
Trnkoczy, A., 2002. Understanding and Parameter Setting of STA/LTA Trigger Algorithm. IASPEI New Manual of Seismological Observatory Practice. 2, pp. 1–19.
Tsuboi, C., 1954. Determination of Gutenberg-Richter's magnitude of earthquakes occurring in and near Japan. Zisin 7, 185–193 (in Japanese).
Tsumura, K., 1967. Determination of earthquake magnitude from total duration of oscillation. Bull. Earthq. Res. Ins. 45, 7–18.
Utsu, T., Ogata, Y., Matsuura, R.S., 1995. The centenary of the Omori formula for a decay law of aftershock activity. J. Phys. Earth 43, 1–33.
Velasco, A.A., Hernandez, S., Parsons, T., Pankow, K., 2008. Global ubiquity of dynamic earthquake triggering. Nat. Geosci. 1, 375–379.
Waldhauser, F., Ellsworth, W.L., 2000. A double-difference earthquake location algorithm: method and application to the northern Hayward fault, California. Bull. Seismol. Soc. Am. 90, 1353–1368.
West, M., Sanchez, J.J., McNutt, S.R., 2005. Periodically triggered seismicity at Mount Wrangell, Alaska, after the Sumatra earthquake. Science 308, 1144–1146.

Wiemer, S., Wyss, M., 2000. Minimum magnitude of completeness in earthquake catalogs: examples from Alaska, the western United States, and Japan. Bull. Seismol. Soc. Am. 90, 859–869.

Withers, M., Aster, R., Young, C., 1999. An automated local and regional seismic event detection and location system using waveform correlation. Bull. Seismol. Soc. Am. 89, 657–669.

Wu, C., Peng, Z., Wang, W., Chen, Q.F., 2011. Dynamic triggering of shallow earthquakes near Beijing, China. Geophys. J. Int. 185, 1321–1334.

Yagi, Y., Fukahata, Y., 2011. Rupture process of the 2011 Tohoku-oki earthquake and absolute elastic strain release. Geophys. Res. Lett. 38, L19307. http://dx.doi.org/10.1029/2011GL048701.

Yukutake, Y., Honda, R., Harada, M., Aketagawa, T., Ito, H., Yoshida, A., 2011. Remotely-triggered seismicity in the Hakone volcano following the 2011 off the Pacific coast of Tohoku earthquake. Earth Planets Space 63, 737–740.

Yukutake, Y., Miyazawa, M., Honda, R., Harada, M., Ito, H., Sakaue, M., Koketsu, K., Yoshida, A., 2013. Remotely triggered seismic activity in Hakone volcano during and after the passage of surface waves from the 2011 M9.0 Tohoku-Oki earthquake. Earth Planet. Sci. Lett. 373, 205–216.

Zhou, X., Sun, W., Zhao, B., Fu, G., Dong, J., Nie, Z., 2012. Geodetic observations detecting coseismic displacements and gravity changes caused by the Mw = 9.0 Tohoku-Oki earthquake. J. Geophys. Res. 117, B05408. http://dx.doi.org/10.1029/2011JB008849.